RESEARCH ARTICLE

Check for updates

Supramolecular nanoparticles constructed from pillar[5]arene-based host–guest complexation with enhanced aggregation-induced emission for imaging-guided drug delivery†

Dahai Liu, [iD] [a] Jianshi Du,[a] Shaolong Qi,[a] Mengyao Li,[a] Jianfeng Wang,*[b] Meihan Liu,*[c] Xianlong Du,[d] Xinyu Wang,[a] Bichen Ren,[a] Dan Wu[e] and Jie Shen [iD] *[f]

Fluorophores with aggregation-induced emission (AIE) characteristics have attracted more and more attention due to their unparalleled advantages in terms of sensitivity and photostability, and have been extensively utilized for disease diagnosis and therapy. However, it remains challenging to restrict the intramolecular rotation of the AIE luminogens (AIEgens) both in solution and aggregated states. Herein, we utilize host–guest chemistry to achieve this meaningful goal by using a carboxylate-modified pillar[5]arene **H** as a supramolecular host and an AIEgen containing a tetraphenylethene core **G** as a guest. The AIE effect of the fluorophore is effectively enhanced upon the formation of an inclusion host–guest complex **H⊃G**, and the fluorescence of **H⊃G** is much more intensive than that of free **G**. Supramolecular nanoparticles (**SNPs**) with high emission are prepared from **H⊃G** using a nanoprecipitation method, which can be used as a fluorescent probe for living cell imaging showing superior photostability against laser excitation. Intriguingly, the formed **SNPs** act as nanocarriers to encapsulate doxorubicin (DOX) to deactivate both the fluorescence of **SNPs** and DOX caused by the energy transfer relay (ETR) effect, which is mediated by Förster resonance energy transfer and aggregation-caused quenching. The release of loaded DOX after cellular internalization interrupts the ETR effect to light up the silenced fluorescence, thus allowing *in situ* visualization of drug release. More importantly, the anticancer efficacy of the loaded drug is greatly maintained using this sophisticated supramolecular system, showing promising potential in imaging-guided drug delivery.

Introduction

Fluorophores, such as cyanine, 2,1,3-benzothiadiazole, rhodamine, fluorescein and boron-dipyrromethene dyes with bright emission have been demonstrated as promising fluorescent probes and even therapeutic agents for biological and biomedical applications.[1–8] Typically, these fluorophores work in very dilute states due to the aggregation-caused quenching (ACQ) effect whose emissions are significantly quenched at high concentration or in the aggregate state, arising from the formation of excimers and exciplexes in the condensed phase mainly triggered by the intermolecular π–π stacking and hydrophobic interactions.[9–13] As a consequence, their fluorescence signals are easily photobleached when harsh laser beams are applied as the excitation light sources, which greatly undermines their sensitivity and poses formidable hurdles for further utilization.[14–20] In sharp comparison to the ACQ effect, novel organic luminogens with an extraordinary aggregation-induced emission (AIE) behavior have been developed and attracted wide attention over the past few years.[21–27] With tetraphenylethene (TPE) and hexaphenylsilole being typical examples, these AIE luminogens (AIEgens) are poorly emissive in solution while become intensely fluorescent on molecular aggregation.[28–33] The mechanism behind this phenomenon is involved in the restriction of intramolecular rotation (RIR) of the aromatic rings, which is exactly opposite to the ACQ systems.[34–40] More importantly, the AIEgen-based fluorophores exhibit unique advantages in photostability that are more resistant to laser irradiations.

[a] *Lymph and Vascular Surgery Department, China-Japan Union Hospital of Jilin University, Changchun, Jilin, 130033, P. R. China*

[b] *Department of Radiotherapy, China-Japan Union Hospital of Jilin University, Changchun, Jilin, 130033, P. R. China. E-mail: jfwang@jlu.edu.cn*

[c] *Department of Ultrasonography, China-Japan Union Hospital of Jilin University, Changchun, Jilin, 130033, P. R. China. E-mail: meihan@jlu.edu.cn*

[d] *School of Pharmaceutical Science, Jilin University, Changchun, Jilin, 130033, P. R. China*

[e] *Department of Chemistry, Institute of Chemical Biology and Pharmaceutical Chemistry, Zhejiang University, Hangzhou 310027, P. R. China*

[f] *School of Medicine, Zhejiang University City College, Hangzhou 310015, P. R. China. E-mail: shenj@zucc.edu.cn*

† Electronic supplementary information (ESI) available: Details of synthesis procedures, NMR spectra and other supplementary information. See DOI: 10.1039/d0qm00974a

For some special biomedical and theranostic applications requiring fluorophores with high sensitivity and contrast, it is extremely important to fabricate new AIEgens whose fluorescence brightly emits even in dilute solution. We anticipated that encapsulating AIE-type chromophores within a rigid cavity would provide a sophisticated strategy to effectively restrict the phenyl rotation at the molecular level, thus achieving the AIE effect. Macrocycles including cyclodextrins, cucurbiturils, calixarenes and pillararenes are brilliant supramolecular hosts with the ability to wrap guest molecules in their inner cavity upon the formation of inclusion complexes,[41–49] providing feasible platforms to reduce the intramolecular rotation of the AIEgens by taking advantage of non-covalent interactions. Benefiting from their highly symmetrical and rigid pillar architectures, versatile functionalizations, and fantastic host–guest recognitions, pillar[n]arenes have attracted more and more attention from scientists since their discovery.[50–54] Fruitful supramolecular systems, including supramolecular polymers, sensors, liquid crystals, molecular machines, drug delivery systems, metal–organic frameworks and theranostic agents, have been successfully constructed by exploiting their outstanding properties.[55–61] However, the fabrications of AIE-based nanomaterials with multiple functions exploiting the pillar[n]arenes-based platforms is scant.

Herein, we prepare supramolecular nanoparticles with enhanced AIE effect by employing pillar[5]arene-based host–guest complexation and further utilize them as fluorescent nanocarriers for imaging-guided drug delivery (Scheme 1). A pillar[5]arene modified by one carboxylate group (H) is used as a supramolecular host and a TPE-cored chromophore containing a pyridine (G) as a supramolecular guest. The fluorescence intensity of G significantly bursts by restricting the intramolecular rotation of G upon the formation of the inclusion complex H⊃G mainly driven by the proton transfer-assisted electrostatic interactions. Through a nanoprecipitation method, supramolecular nanoparticles (SNPs) possessing bright emission are obtained, of which photostability is remarkably high. More interestingly, a dual-fluorescence-quenched ternary system SNPs@DOX is constructed by loading an anticancer drug doxorubicin (DOX) into the SNPs caused by the energy transfer relay (ETR) effect, which is mediated by Förster resonance energy transfer (FRET) from the SNPs to DOX followed by the ACQ effect. Triggered by low intracellular pH, the loaded DOX molecules effectively release from the SNPs@DOX, and thus the silenced fluorescence is fully recovered by interrupting the ETR effect. Benefiting from the AIE effect and non-covalent interactions, this supramolecular system will possibly be applied in imaging-guided drug delivery, allowing visualization of the drug release in real-time.

Results and discussion

^{1}H NMR spectroscopy was utilized to study the host–guest recognition between H and G (Fig. 1). In order to eliminate the influence on the chemical shifts caused by the protonation and deprotonation during host–guest complexation, we utilized M and deprotonated pillar[5]arene (H′) as model compounds so that the non-covalent interactions could be monitored by detecting the chemical shift changes before and after complexation. Compared with the proton signals of free M, apparent changes in chemical shifts related to the protons on M were observed upon the addition of H′ (Fig. 1a and b). The signals of protons H_e and H_d displayed an upfield shift after host–guest complexation ($\Delta\delta$ = 0.283 and 0.061 ppm for H_e and H_d, respectively), indicating that the guest deeply penetrated into the cavity of H′ and these protons were shielded by the electron-rich cyclic structure upon the formation of an inclusion complex.[62] In addition, a broadening effect was observed for these peaks caused by the complexation dynamics (Fig. 1b). In addition, slight chemical shift changes were also observed for the peaks related to the protons H_1 and H_{1*} ($\Delta\delta$ = 0.008 and 0.014 ppm for H_1 and H_{1*}, respectively), which was caused by the host–guest complexation. 2D NOESY NMR spectroscopy was used to reveal the topological structure and relative position of the building blocks in the host–guest complex H′⊃M (Fig. 1d). Intensive nuclear Overhauser effect correlations between the peaks of protons ($H_{a–e}$) and protons (H_1 and H_{1*}) were observed, which further indicated that M penetrated into the cavity of the cyclic pillar[5]arene host through host–guest interactions.

In order to reveal the complexation thermodynamic behaviors and binding affinity of H⊃G, an isothermal titration calorimetry (ITC) experiment was conducted (Fig. 2). The association constant was measured to be $(1.27 \pm 0.10) \times 10^4$ M^{-1} with a 1:1 complexation stoichiometry. Moreover, the changes in enthalpy and entropy were also calculated from ITC measurement to be −14.1 kJ mol^{-1} and 31.2 J mol^{-1} deg^{-1}, respectively, which indicated that the host–guest recognition was driven by advantageous entropy changes with the assistance of enthalpy.[63] Direct evidence for the formation of H⊃G came from electrospray ionization mass spectrometry, in which a peak at m/z 1204.4 was detected corresponding to [H⊃G + H]$^+$, which confirmed the 1:1 complexation between H and G (Fig. S7, ESI†). For H and G, the proton from the carboxylic acid group on H could transfer to the pyridine unit on G in the principle of undergoing an acid–base reaction, thus forming stable electrostatic interaction between H and G that mainly drove the formation of a host–guest complex.

After establishment of the host–guest complexation, the photophysical properties of free G and H⊃G were studied. The AIEgen-based guest G displayed a classical AIE effect. The fluorescence intensity of G was extremely weak in acetone where it was well dissolved. It should be noted that the emission of G in acetone significantly improved in the presence of H attributed to the host–guest interactions (Fig. 3a and b). Under a UV lamp at 365 nm, the yellow emission of the solution G lighted up in the presence of H (Fig. 3b), further supporting the proposed mechanism shown in Fig. 3a. Gradually enhancing the volume fraction of water (f_w) in the mixture of acetone and H_2O from 0 to 80 vol%, the fluorescence intensity of G at 550 nm increased slowly. A dramatic enhancement of the fluorescence intensity was monitored by further improving
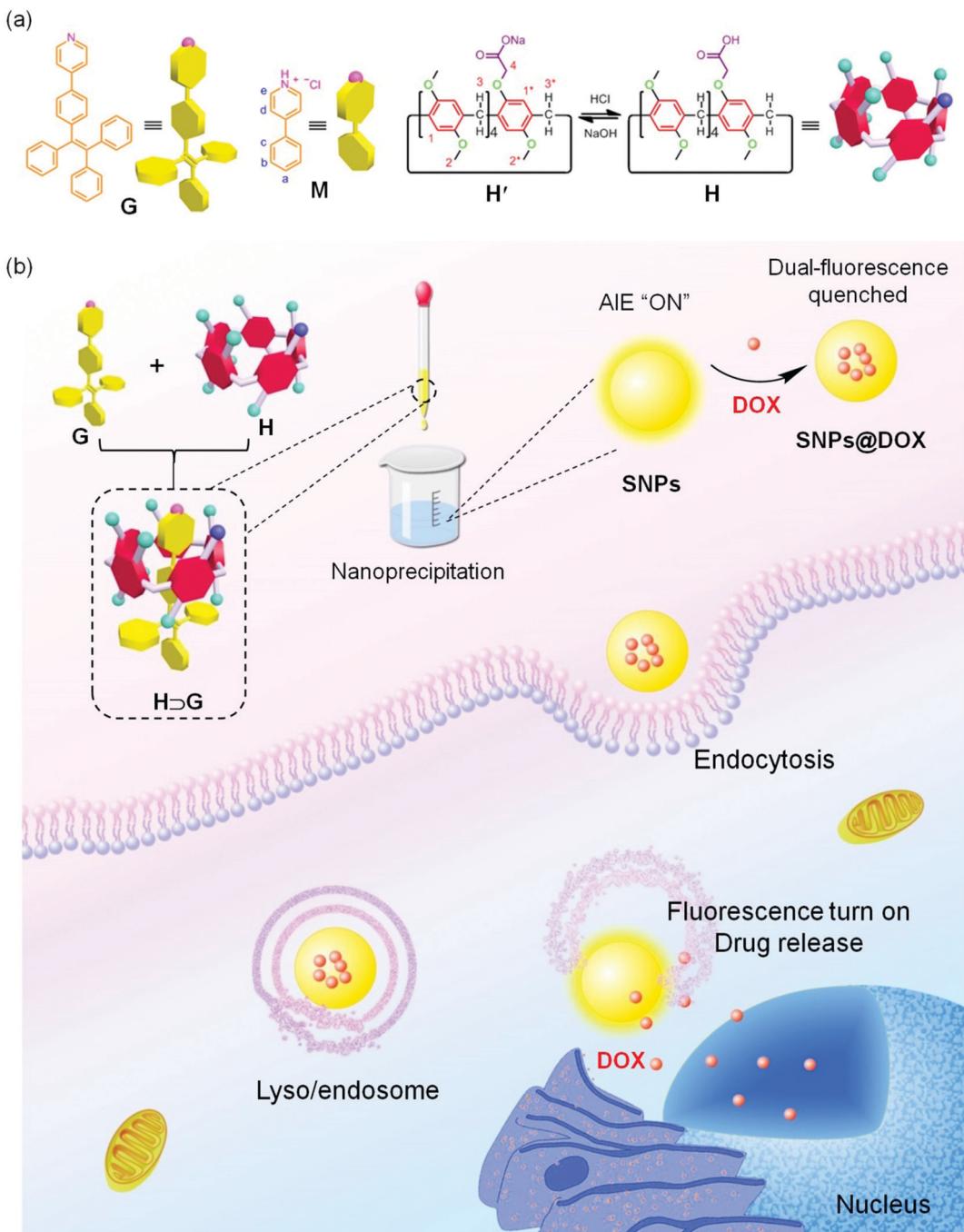
Scheme 1 (a) Chemical structures and cartoon representations of **G**, **M**, and **H**. (b) The fabrication of **SNPs@DOX** using **SNPs** as drug nanocarriers and cartoon illustration of imaging-guided drug delivery. **SNPs** are prepared from the host–guest complex **H⊃G** through a nanoprecipitation method. After cellular endocytosis, the dual-fluorescence quenched nanoparticles **SNPs@DOX** are transported into the lyso/endosome, where the loaded drug releases from **SNPs** due to the protonation of DOX in an acidic microenvironment, thus recovering the fluorescence.

the f_w value from 80 to 98 vol% (Fig. 3e). This phenomenon was consistent with other classical AIE dyes. Excitingly, the AIE property was maintained by the formation of **H⊃G** and a complexation-triggered enhancement of the AIE effect was achieved (Fig. 3c and Fig. S8, ESI†). As shown in Fig. 3e, the fluorescence intensity of **H⊃G** was always much higher than that of **G** at the same f_w values. The emission intensity of **H⊃G**

was around 2.8 times that of free **G** when f_w reached 98% (Fig. 3c). The mechanism behind the complexation-enhanced AIE effect was that the intramolecular rotation of **G** was significantly restricted by the formation of a [2]psedorotaxane-type structure (Fig. 3a). The nonradiative decay channels of the AIEgen-based guest were effectively blocked, thus bursting the fluorescent emission. In addition, the hydrophobicity of
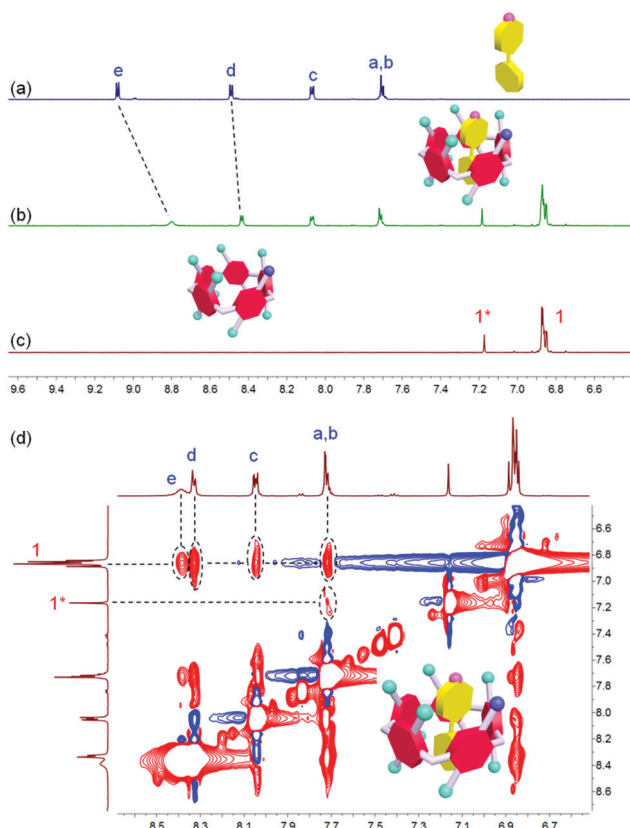
Fig. 1 Partial ^{1}H NMR spectra (400 MHz, acetone-d_6/D$_2$O = 1:1, room temperature) of (a) **M** (1.00 mM), (b) **H′** (1.00 mM) and **M** (1.00 mM), and (c) **H′** (1.00 mM). (d) Partial NOESY NMR spectrum (400 MHz, acetone-d_6/D$_2$O = 1:1, room temperature) of **H′⊃M** (5.00 mM).

Fig. 2 ITC data of the host–guest complexation between **H′** and **M** at 298.15 K.

the AIE-active fluorogen was remarkably increased by incorporating hydrophobic **H** into this supramolecular complex, which was also favourable to promote the AIE effect by improving the aggregation of **H⊃G** in aqueous solution.

In order to improve the stability of the host–guest complex for biomedical applications, **SNPs** were prepared through a nano-precipitation method by slowly adding the acetone solution of **H⊃G** into water under sonication. As shown in the transmission electron microscopy (TEM) image, spherical nanoparticles with a diameter ranging from 50 to 110 nm were observed (Fig. 3d). The average diameter of these nanoparticles was determined by dynamic light scattering (DLS) to be 87.3 ± 7.9 nm (Fig. 3f), in good agreement with the result obtained from TEM. The stability of the **SNPs** in the physiological environment was evaluated by DLS measurements, and negligible changes in mean diameter were detected in PBS within 24 h (Fig. S9, ESI†), ensuring the biomedical applications of **SNPs**.

The internalization pathways of the **SNPs** were investigated by using various endocytosis inhibitors. Cellular uptake of **SNPs** by U87MG cells was significantly blocked at 4 °C, demonstrating that the cellular uptake was energy-dependent. Additionally, the endocytosis of **SNPs** was greatly inhibited in the presence of amiloride-HCl (AMD), chlorpromazine (CPZ) or genistein (Gen). Pre-treatment of the cells with AMD, CPZ or Gen resulted

in 23.7%, 51.1% or 22.9% reduction in the cellular internaliza-tion (Fig. 4a), respectively, which indicated that the **SNPs** were internalized mainly through the clathrin-mediated endocytic pathway with the assistance of macropinocytosis- and caveolae-mediated uptake.[64,65] These internalization pathways allowed **SNPs** to undergo an endo/lysosomal transportation for intracellular delivery. A 3-(4′,5′-dimethyl-2′-thiazolyl)-2,5-diphenyltetrazolium bromide (MTT) assay was utilized to assess the cytotoxicity of **SNPs**. Incubation with **H**, **G**, or **SNPs** for 24 h led to ignorable influence on relative cell viability against both cancerous U87MG and normal HEK293 cells (Fig. S10 and S11, ESI†), a convincing indicator of excellent biocompatibility of these building blocks and the supramolecular complex for biomedical use.

Confocal laser scanning microscopy (CLSM) was utilized to reveal the cellular internalization of **SNPs** and trace their intracellular location. As shown in Fig. 4b, yellow fluorescence was observed in the cytoplasm after 4 h incubation with **SNPs**, and the signal was well-overlapped with the red fluorescence from LysoTracker Red (LysoRed), suggesting that **SNPs** mainly accumu-lated in lyso/endosomes after endocytosis. More intriguingly, the **SNPs** displayed superior photostability under laser excitation during cell imaging. CLSM images indicated that the fluorescence of **SNPs** was greatly maintained after 30 scans, and only 5.8% signal loss was determined (Fig. 4c and d). In sharp comparison, the fluorescence signal of LysoRed almost vanished after 15 scans with a signal loss as high as 78.4% (Fig. 4c and Fig. S12, ESI†), because LysoRed was easily quenched at low working concen-tration by laser excitation. For **SNPs**, although their outermost layer was possibly photobleached upon exposure to a laser,

This journal is © The Royal Society of Chemistry and the Chinese Chemical Society 2021

Mater. Chem. Front., 2021, **5**, 1418–1427 | **1421**
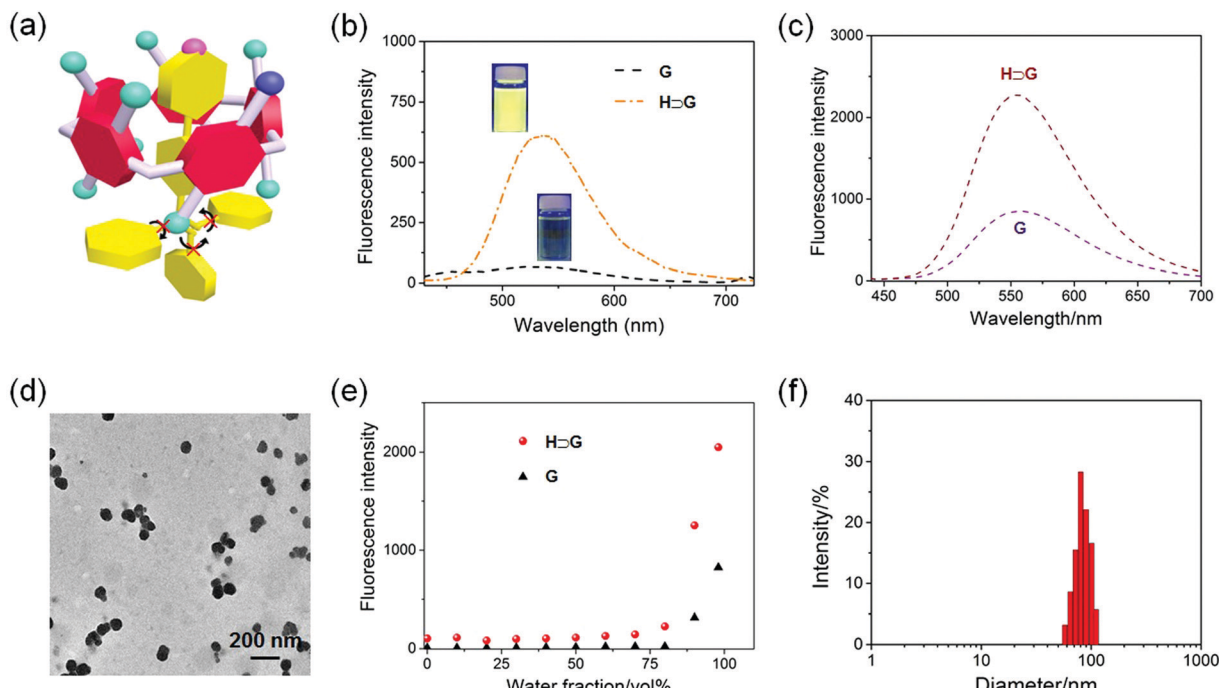
Fig. 3 (a) Cartoon representation of complexation–induced AIE enhancement by restricting the intramolecular rotation of **G**. (b) Fluorescence spectra of **G** (100 μM) and **H⊃G** (100 μM) in acetone. Inset: The photos of the corresponding solution under UV lamp. (c) Fluorescence spectra of **G** (5.00 μM) and **H⊃G** (5.00 μM) in aqueous solution. (d) TEM image of **SNPs** prepared from **H⊃G**. (e) Plots of the emission intensity at 550 nm *versus* f_w of the aqueous mixtures containing **G** (5.00 μM) and **H⊃G** (5.00 μM), respectively. (f) DLS result of the solution containing **SNPs**.
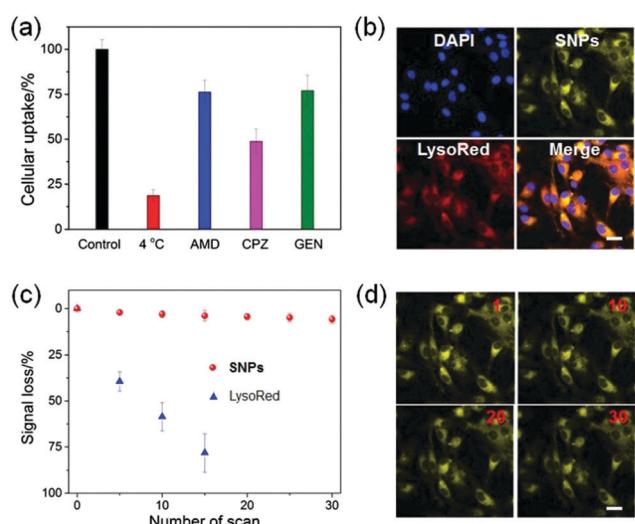
Fig. 4 (a) Cellular internalization of **SNPs** in the absence and presence of various inhibitors. (b) CLSM images of U87MG cells after 4 h incubation with **SNPs**. (c) Signal loss of fluorescent emission of **SNPs** and LysoTracker Red with increasing number of scans. (d) CLSM images of U87MG cells stained with **SNPs** with increasing number of scans (the number of scans is shown in the upper right corner).

the nanoparticle structure helped to avoid photo-oxidization due to the resistance of oxygen diffusion into the cores, thus significantly improving the photostability of **SNPs**.

Considering the hydrophobicity of this binary supramolecular system, **SNPs** could be further utilized as nanocarriers to

encapsulate anticancer drugs driven by π–π stacking and hydrophobic interactions between the drug and **H⊃G**. Indeed, DOX could be encapsulated into **SNPs** to form a ternary delivery system (**SNPs@DOX**) with a drug loading content of 26.7%. Negligible changes in morphology were observed after loading DOX (Fig. S13, ESI†), and only a slight increase in the mean diameter was detected for **SNPs@DOX** with an average diameter of 104 nm (Fig. S14, ESI†). The successful encapsulation was further confirmed by zeta potential measurements, in which the zeta value increased from −7.8 mV for **SNPs** to 23.2 mV for **SNPs@DOX** (Fig. S15 and S16, ESI†).

Interestingly, a huge overlap was detected between the absorption of DOX and the emission of **SNPs** (Fig. 5a), suggesting that a FRET process could take place in **SNPs@DOX**, in which the AIEgen **G** worked as a fluorescent donor and anticancer drug DOX acted as an acceptor. As shown in Fig. 5b, the emission intensity at around 550 nm corresponding to the characteristic fluorescence of **SNPs** weakened upon the gradual addition of DOX. The disappearance of the AIE behavior in the presence of DOX arose from the FRET from TPE-based fluorogens to DOX,[66] because the intermolecular distance between **G** and DOX was close in the hydrophobic core of **SNPs@DOX**. Additionally, the fluorescence of DOX self-quenched due to the ACQ effect, which was fundamentally caused by the π–π stacking of DOX molecules with a rigid planar structure. Therefore, a dual-fluorescence-quenched drug delivery system was constructed on the basis of the ETR effect, which was mediated by the FRET and ACQ effects.

The neutral DOX in **SNPs@DOX** could be protonated in an acidic intracellular environment, facilitating its release from
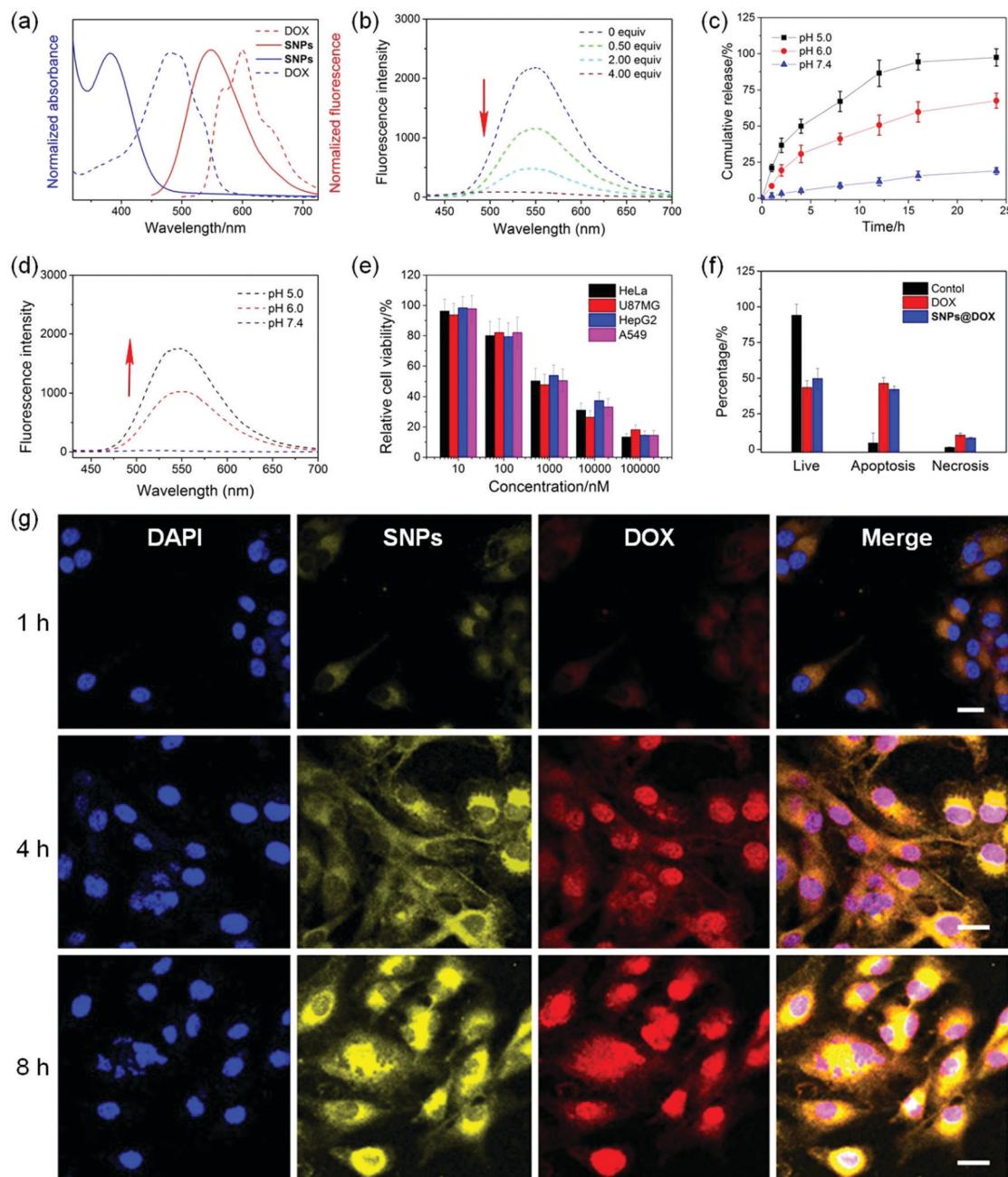
Fig. 5 (a) Absorption and fluorescence emission spectra of SNPs and DOX. (b) Fluorescence spectra of **SNPs** in the presence of different amounts of DOX. (c) Drug release curves of **SNPs@DOX** under different pH values. (d) Fluorescence recovery of **SNPs@DOX** after 8 h incubation under different pH values. (e) Relative cell viability of **SNPs@DOX** against various cell lines at different concentrations after 24 h incubation. (f) Apoptosis analysis of the U87MG cells treated with different formulations. (g) CLSM images of the U87MG cells incubated with **SNPs@DOX** for 1 h, 4 h and 8 h, respectively. Scale bars = 25 μm.

the nanoformulation to activate its anticancer capability. In order to mimic the pH gradient from the bloodstream to the intracellular endo/lysosome, the release behaviors of DOX from **SNPs@DOX** were measured at pH 7.4, 6.0, and 5.0, respectively. Fig. 5c indicated that the release profile was pH-dependent. The ternary system was quite stable at pH 7.4, and only 18.2% of the loaded DOX was released within 24 h incubation. The release rate and amount greatly accelerated in an acidic environment, and 67.5% of the loaded DOX was released from **SNPs@DOX** at

pH 6.0 and 95.4% at pH 5.0 within the same period. More importantly, the ETR effect between **SNPs** and DOX was interrupted accompanied by the release of DOX, thus recovering the fluorescence of the **SNPs** (Fig. 5d). Therefore, the drug release process could be traced in real-time by detecting the magnitude and location of the energy transfer-dependent fluorescent variations, allowing imaging-guided drug delivery.

CLSM was used to study the internalization and *in situ* drug release behaviour of **SNPs@DOX**. After 1 h of incubation with

This journal is © The Royal Society of Chemistry and the Chinese Chemical Society 2021

Mater. Chem. Front., 2021, **5**, 1418–1427 | **1423**

SNPs@DOX, yellow fluorescence from **SNPs** and red fluorescence from DOX was found in the cytoplasm of the U87MG cells (Fig. 5g). The fluorescence signals became much more intensive by extending the incubation time to 4 h, which demonstrated that the loaded DOX successfully escaped from **SNPs@DOX**. Attributed to the nucleus-targeting ability of DOX, the released anticancer drug entered into the cell nucleus, as evidenced by the colocolization of blue fluorescence from DAPI and red fluorescence from DOX. The fluorescence intensity of **SNPs** and DOX further increased after 8 h incubation, and most of the drug translocated into the nucleus where its anticancer activity took place. After being internalized by the cancer cells, **SNPs@DOX** was transported into the endo/lysosomes with a relatively low pH, where the neutral DOX could be protonated into the cationic state, leading to the release of loaded DOX from **SNPs@DOX**. As a result, the silenced fluorescence "woke up" by interrupting the ETR effect between the **SNPs** and DOX.

The MTT assay was employed to evaluate the anticancer efficacy of **SNPs@DOX**, and free DOX was chosen as a control. Significant growth inhibition was observed for various cancer cell lines treated with **SNPs@DOX** at a high DOX concentration, including HeLa, U87MG, HepG2, and A549 cells. According to the MTT assay, the half maximal inhibitory concentrations (IC_{50}) of **SNPs@DOX** were calculated to be 2.14 ± 0.17, 1.80 ± 0.11, 2.88 ± 0.20, and 1.96 ± 0.14 μM against HeLa, U87MG, HepG2, and A549 cells, respectively. The anticancer efficacy of **SNPs@DOX** was comparable to that of free DOX, whose IC_{50} values were 3.25 ± 0.28, 1.77 ± 0.14, 2.63 ± 0.18, and 1.53 ± 0.10 μM against HeLa, U87MG, HepG2, and A549 cells, respectively (Fig. S18, ESI†). The quantities of living cells, apoptosis cells, and necrosis cells were determined after the U87MG cells were administrated with free DOX and **SNPs@DOX**. The corresponding apoptotic and necrotic cell counts in these two therapeutic groups were very close, in good agreement with the results obtained from the MTT assay. Similarly, **SNPs** could be used as feasible nanocarriers to load other hydrophobic anticancer drugs, such as camptothecin and paclitaxel. Compared with the free drugs, the potency of these supramolecular drug delivery systems was greatly maintained benefiting from the non-covalent interactions (Fig. S19–S26, ESI†). These studies demonstrated that the supramolecular system possessing AIE properties showed promising potential in imaging-guided drug delivery.[67–69]

Conclusions

In summary, we established a new host–guest recognition between a carboxylate-modified pillar[5]arene **H** and a TPE-based guest **G**. The intramolecular rotation of the aromatic rings of **G** was effectively restricted after the formation of **H ⊃ G**, in which the pyridine head deeply penetrated into the cavity of **H** driven by the electrostatic interaction. Benefiting from the complexation-enhanced AIE effect, highly emissive **SNPs** were prepared, which could be used for living cell imaging with excellent photostability. More interestingly, **SNPs** were able to load DOX to afford a self-imaging drug delivery system.

Mediated by FRET and ACQ effects, the fluorescence from **SNPs** and DOX were both extinguished arising from the ETR effect. The release of loaded DOX from **SNPs@DOX** woke up the silenced fluorescence triggered in an acidic microenvironment, which allowed the *in situ* detection of drug release in cells. *In vitro* studies verified that the anticancer capability of the drugs in the nanoformulations was effectively preserved using this supramolecular nanomaterial. The present study provides a novel supramolecular method for the construction of imaging-guided drug delivery systems, which have great potential applications in the field of cancer treatment.

Author contributions

D. Liu, J. Wang, M. Liu, D. Wu, and J. Shen conceived and designed the research. D. Liu, S. Qi, M. Li, and D. Wu synthesized the compounds and investigated the host–guest complexation. D. Liu, X. Du, X. Wang, B. Ren, M. Liu, and J. Shen conducted the *in vitro* studies. D. Liu, J. Wang, M. Liu, D. Wu, and J. Shen co-wrote the paper.

Conflicts of interest

The authors declare no competing financial interest.

Acknowledgements

Notes and references

1 R. Weissleder and M. J. Pittet, Imaging in the era of molecular oncology, *Nature*, 2008, **452**, 580–589.
2 E. Meijering, A. E. Carpenter, H. Peng, F. A. Hamprecht and J.-C. Olivo-Marin, Imagining the future of bioimage analysis, *Nat. Biotechnol.*, 2016, **34**, 1250–1255.
3 J. R. W. Conway, N. O. Carragher and P. Timpson, Developments in preclinical cancer imaging: innovating the discovery of therapeutics, *Nat. Rev. Cancer*, 2014, **14**, 314–328.
4 A. L. Antaris, H. Chen, K. Cheng, Y. Sun, G. Hong, C. Qu, S. Diao, Z. Deng, X. Hu, B. Zhang, X. Zhang, O. K. Yaghi, Z. R. Alamparambil, X. Hong, Z. Cheng and H. Dai, A small-molecule dye for NIR-II imaging, *Nat. Mater.*, 2016, **15**, 235–242.
5 G. Hong, A. Antaris and H. Dai, Near-infrared fluorophores for biomedical imaging, *Nat. Biomed. Eng.*, 2017, **1**, 0010.
6 M. Gao, F. Yu, C. Lv, J. Choo and L. Chen, Fluorescent chemical probes for accurate tumor diagnosis and targeting therapy, *Chem. Soc. Rev.*, 2017, **46**, 2237–2271.

7 D. Wang and B. Z. Tang, Aggregation-induced emission luminogens for activity-based sensing, *Acc. Chem. Res.*, 2019, **52**, 2559–2570.

8 J. Mei, N. L. C. Leung, R. T. K. Kwok, J. W. Y. Lam and B. Z. Tang, Aggregation-induced emission: together we shine, united we soar!, *Chem. Rev.*, 2015, **115**, 11718–11940.

9 S. Wang, Y. Fan, D. Li, C. Sun, Z. Lei, L. Lu, T. Wang and F. Zhang, *Nat. Commun.*, 2019, **10**, 1058.

10 H.-B. Cheng, Y. Li, B. Z. Tang and J. Yoon, *Chem. Soc. Rev.*, 2020, **49**, 21–31.

11 Y. Li, S. Liu, T. Han, H. Zhang, C. Chuah, R. T. K. Kwok, J. W. Y. Lam and B. Z. Tang, Sparks fly when AIE meets with polymers, *Mater. Chem. Front.*, 2019, **3**, 2207–2220.

12 J. Mei, Y. Hong, J. W. Y. Lam, A. Qin, Y. Tang and B. Z. Tang, Aggregation-induced emission: the whole is more brilliant than the parts, *Adv. Mater.*, 2014, **26**, 5429–5479.

13 P. Gao, W. Pan, N. Li and B. Tang, Fluorescent probes for organelle-targeted bioactive species imaging, *Chem. Sci.*, 2019, **10**, 6035–6071.

14 G. Feng and B. Liu, Aggregation-induced emission (AIE) dots: emerging theranostic nanolights, *Acc. Chem. Res.*, 2018, **51**(6), 1404–1414.

15 Z. Zhang, Z. Zhao, L. Wu, S. Lu, S. Ling, G. Li, L. Xu, L. Ma, Y. Hou, X. Wang, X. Li, G. He, K. Wang, B. Zou and M. Zhang, Emissive platinum(II) cages with reverse fluorescence resonance energy transfer for multiple sensing, *J. Am. Chem. Soc.*, 2020, **142**, 2592–2600.

16 G. Yu, R. Zhao, D. Wu, F. Zhang, L. Shao, J. Zhou, J. Yang, G. Tang, X. Chen and F. Huang, Pillar[5]arene-based amphiphilic supramolecular brush copolymers: fabrication, controllable self-assembly and application in self-imaging targeted drug delivery, *Polym. Chem.*, 2016, **7**, 6178–6188.

17 P. Zhang, X. Nie, M. Gao, F. Zeng, A. Qin, S. Wu and B. Z. Tang, A highly selective fluorescent nanoprobe based on AIE and ESIPT for imaging hydrogen sulfide in live cells and zebrafish, *Mater. Chem. Front.*, 2017, **1**, 838–845.

18 X. Gao, G. Feng, P. N. Manghnani, F. Hu, N. Jiang, J. Liu, B. Liu, J. Z. Sun and B. Z. Tang, A two-channel responsive fluorescent probe with AIE characteristics and its application for selective imaging of superoxide anions in living cells, *Chem. Commun.*, 2017, **53**, 1653–1656.

19 M. Li, Y. Gao, Y. Yuan, Y. Wu, Z. Song, B. Z. Tang, B. Liu and Q. C. Zheng, One-step formulation of targeted aggregation-induced emission dots for image-guided photodynamic therapy of cholangiocarcinoma, *ACS Nano*, 2017, **11**, 3922–3932.

20 D. Wang and B. Z. Tang, Aggregation-induced emission luminogens for activity-based sensing, *Acc. Chem. Res.*, 2019, **52**, 2559–2570.

21 G. Jin, G. Feng, W. Qin, B. Z. Tang, B. Liu and K. Li, Multifunctional organic nanoparticles with aggregation-induced emission (AIE) characteristics for targeted photodynamic therapy and RNA interference therapy, *Chem. Commun.*, 2016, **52**, 2752–2755.

22 D. Ding, K. Li, B. Liu and B. Z. Tang, Bioprobes based on AIE fluorogens, *Acc. Chem. Res.*, 2013, **46**, 2441–2453.

23 G. Yu, M. Zhang, M. L. Saha, Z. Mao, J. Chen, Y. Yao, Z. Zhou, Y. Liu, C. Gao, F. Huang, X. Chen and P. J. Stang, Antitumor activity of a unique polymer that incorporates a fluorescent self-assembled metallacycle, *J. Am. Chem. Soc.*, 2017, **139**, 15940–15949.

24 X. Yan, P. Wei, Y. Liu, M. Wang, C. Chen, J. Zhao, G. Li, M. L. Saha, Z. Zhou, Z. An, X. Li and P. J. Stang, Endo- and exo-functionalized tetraphenylethylene $M_{12}L_{24}$ nanospheres: fluorescence emission inside a confined space, *J. Am. Chem. Soc.*, 2019, **141**, 9673–9679.

25 R. Zhang, G. Niu, Q. Lu, X. Huang, J. H. C. Chau, R. T. K. Kwok, X. Yu, M.-H. Li, J. W. Y. Lam and B. Z. Tang, Cancer cell discrimination and dynamic viability monitoring through wash-free bioimaging using AIEgens, *Chem. Sci.*, 2020, **11**, 7676–7684.

26 Y. Gao, H. Zhang, Z. He, F. Fang, C. Wang, K. Zeng, S. Gao, F. Meng, L. Luo and B. Z. Tang, Multicationic AIEgens for unimolecular photodynamic theranostics and two-photon fluorescence bioimaging, *Mater. Chem. Front.*, 2020, **4**, 1623–1633.

27 G. Yu, G. Tang and F. Huang, Supramolecular enhancement of aggregation-induced emission and its application in cancer cell imaging, *J. Mater. Chem. C*, 2014, **2**, 6609–6617.

28 D. Wu, Y. Li, J. Yang, J. Shen, J. Zhou, Q. Hu, G. Yu, G. Tang and X. Chen, Supramolecular nanomedicine constructed from cucurbit[8]uril-based amphiphilic brush copolymer for cancer therapy, *ACS Appl. Mater. Interfaces*, 2017, **9**(51), 44392–44401.

29 Y. Liao, B. Li, Z. Zhao, Y. Fu, Q. Tan, X. Li, W. Wang, J. Yin, H. Shan, B. Z. Tang and X. Huang, Targeted theranostics for tuberculosis: a rifampicin-loaded aggregation-induced emission carrier for granulomas tracking and anti-infection, *ACS Nano*, 2020, **14**, 8046–8058.

30 X. Yan, M. Wang, T. R. Cook, M. Zhang, M. L. Saha, Z. Zhou, X. Li, F. Huang and P. J. Stang, Light-emitting superstructures with anion effect: coordination-driven self-assembly of pure tetraphenylethylene metallacycles and metallacages, *J. Am. Chem. Soc.*, 2016, **138**, 4580–4588.

31 G. Yu, D. Wu, Y. Li, Z. Zhang, L. Shao, J. Zhou, Q. Hu, G. Tang and F. Huang, A pillar[5]arene-based [2]rotaxane lights up mitochondria, *Chem. Sci.*, 2016, **7**, 3017–3024.

32 J. Li, K. Shi, M. Drechsler, B. Z. Tang, J. Huang and Y. Yan, A supramolecular fluorescent vesicle based on a coordinating aggregation induced emission amphiphile: insight into the role of electrical charge in cancer cell division, *Chem. Commun.*, 2016, **52**, 12466–12469.

33 J. Shi, Y. Li, Q. Li and Z. Li, Enzyme-responsive bioprobes based on the mechanism of aggregation-induced emission, *ACS Appl. Mater. Interfaces*, 2018, **10**, 12278–12294.

34 D. Wu, L. Shao, Y. Li, Q. Hu, F. Huang, G. Yu and G. Tang, A boron difluoride dye showing the aggregation-induced emission feature and high sensitivity to intra- and extracellular pH changes, *Chem. Commun.*, 2016, **52**, 541–544.

35 G. Yu, T. R. Cook, Y. Li, X. Yan, D. Wu, L. Shao, J. Shen, G. Tang, F. Huang, X. Chen and P. J. Stang, A tetraphenylethene-based highly emissive metallacage as a component of theranostic

This journal is © The Royal Society of Chemistry and the Chinese Chemical Society 2021

Mater. Chem. Front., 2021, **5**, 1418–1427 | **1425**

supramolecular nanoparticles, *Proc. Natl. Acad. Sci. U. S. A.*, 2016, **113**, 13720–13725.

36 J. Qi, X. Duan, Y. Cai, S. Jia, C. Chen, Z. Zhao, Y. Li, H.-Q. Peng, R. T. K. Kwok, J. W. Y. Lam, D. Ding and B. Z. Tang, Simultaneously boosting the conjugation, brightness and solubility of organic fluorophores by using AIEgens, *Chem. Sci.*, 2020, **11**, 8438–8447.

37 L. Yang, W. Fang, Y. Ye, Z. Wang, Q. Hu and B. Z. Tang, Redox-responsive fluorescent AIE bioconjugate with aggregation enhanced retention features for targeted imaging reinforcement and selective suppression of cancer cells, *Mater. Chem. Front.*, 2019, **3**, 1335–1340.

38 W. Qin, N. Alifu, Y. Cai, J. W. Y. Lam, X. He, H. Su, P. Zhang, J. Qian and B. Z. Tang, Synthesis of an efficient far-red/near-infrared luminogen with AIE characteristics for in vivo bioimaging applications, *Chem. Commun.*, 2019, **55**, 5615–5618.

39 C. Zhang, S. Jin, S. Li, X. Xue, J. Liu, Y. Huang, Y. Jiang, W.-Q. Chen, G. Zou and X.-J. Liang, Imaging intracellular anticancer drug delivery by self-assembly micelles with aggregation-induced emission (AIE micelles), *ACS Appl. Mater. Interfaces*, 2014, **6**, 5212–5220.

40 X. Ni, X. Zhang, X. Duan, H.-L. Zheng, X.-S. Xue and D. Ding, Near-infrared afterglow luminescent aggregation-induced emission dots with ultrahigh tumor-to-liver signal ratio for promoted image-guided cancer surgery, *Nano Lett.*, 2019, **19**, 318–330.

41 S. J. Barrow, S. Kasera, M. J. Rowland, J. Barrio and O. A. Scherman, Cucurbituril-based molecular recognition, *Chem. Rev.*, 2015, **115**, 12320–12406.

42 G. Yu, K. Jie and F. Huang, Supramolecular amphiphiles based on host–guest molecular recognition motifs, *Chem. Rev.*, 2015, **115**, 7240–7303.

43 T. Ogoshi, T. Yamagishi and Y. Nakamoto, Pillar-shaped macrocyclic hosts pillar[n]arenes: new key players for supramolecular chemistry, *Chem. Rev.*, 2016, **116**, 7937–8002.

44 M. Xue, Y. Yang, X. Chi, Z. Zhang and F. Huang, Pillararenes, a new class of macrocycles for supramolecular chemistry, *Acc. Chem. Res.*, 2012, **45**, 1294–1308.

45 X. Ji, M. Ahmed, L. Long, N. M. Khashab, F. Huang and J. L. Sessler, Adhesive supramolecular polymeric materials constructed from macrocycle-based host–guest interactions, *Chem. Soc. Rev.*, 2019, **48**, 2682–2697.

46 A. Harada, Cyclodextrin-based molecular machines, *Acc. Chem. Res.*, 2001, **34**, 456–464.

47 J. Zhou, G. Yu and F. Huang, Supramolecular chemotherapy based on host–guest molecular recognition: a novel strategy in the battle against cancer with a bright future, *Chem. Soc. Rev.*, 2017, **46**, 7021–7053.

48 D.-S. Guo and Y. Liu, Supramolecular chemistry of *p*-Sulfonatocalix[n]arenes and its biological applications, *Acc. Chem. Res.*, 2014, **47**, 1925–1934.

49 D. Xia, P. Wang, X. Ji, N. M. Khashab, J. L. Sessler and F. Huang, Functional supramolecular polymeric networks: the marriage of covalent polymers and macrocycle-based host–guest interactions, *Chem. Rev.*, 2020, **120**, 6070–6123.

50 N. L. Strutt, H. Zhang, S. T. Schneebeli and J. F. Stoddart, Functionalizing pillar[n]arenes, *Acc. Chem. Res.*, 2014, **47**, 2631–2642.

51 T. Kakuta, T. Yamagishi and T. Ogoshi, Stimuli-responsive supramolecular assemblies constructed from pillar[n]-arenes, *Acc. Chem. Res.*, 2018, **51**, 1656–1666.

52 H. Zhu, L. Shangguan, B. Shi, G. Yu and F. Huang, Recent progress in macrocyclic amphiphiles and macrocyclic host-based supra-amphiphiles, *Mater. Chem. Front.*, 2018, **2**, 2152–2174.

53 Y. Wang, G. Ping and C. Li, Efficient complexation between pillar[5]arenes and neutral guests: from host–guest chemistry to functional materials, *Chem. Commun.*, 2016, **52**, 9858–9872.

54 J.-D. Ding, W.-J. Jin, Z. Pei and Y. Pei, Morphology transformation of pillararene-based supramolecular nanostructures, *Chem. Commun.*, 2020, **56**, 10113–10126.

55 G. Yu, W. Yu, L. Shao, Z. Zhang, X. Chi, Z. Mao, C. Gao and F. Huang, A pillar[5]arene-based supramolecular diblock copolymeric amphiphile: fabrication and application in Targeted drug delivery, *Adv. Funct. Mater.*, 2016, **26**, 8999–9008.

56 J.-Y. Chen and J.-L. Hou, Controllable synthetic ion channels, *Org. Chem. Front.*, 2018, **5**, 1728–1736.

57 H. Li, D.-X. Chen, Y.-L. Sun, Y. B. Zheng, L.-L. Tan, P. S. Weiss and Y.-W. Yang, Viologen-mediated assembly of and sensing with carboxylatopillar[5]arene-modified gold nanoparticles, *J. Am. Chem. Soc.*, 2013, **135**, 1570–1576.

58 J. Chen, Y. Zhang, Z. Meng, L. Guo, X. Yuan, Y. Zhang, Y. Chai, J. L. Sessler, Q. Meng and C. Li, Supramolecular combination chemotherapy: a pH-responsive co-encapsulation drug delivery system, *Chem. Sci.*, 2020, **11**, 6275–6282.

59 G. Yu, J. Yang, X. Fu, Z. Wang, L. Shao, Z. Mao, Y. Liu, Z. Yang, F. Zhang, W. Fan, J. Song, Z. Zhou, C. Gao, F. Huang and X. Chen, Supramolecular hybrid material constructed from graphene oxide and pillar[6]arene-based host–guest complex as a ultrasound and photoacoustic signals nanoamplifier, *Mater. Horiz.*, 2018, **5**, 429–435.

60 H. Liang, B. Hua, F. Xu, L.-S. Gan, L. Shao and F. Huang, Acid/base-tunable unimolecular chirality switching of a pillar[5]azacrown *pseudo*[1]catenane, *J. Am. Chem. Soc.*, 2020, **142**, 19772–19778.

61 N. L. Strutt, R. S. Forgan, J. M. Spruell, Y. Y. Botros and J. F. Stoddart, Monofunctionalized Pillar[5]arene as a Host for Alkanediamines, *J. Am. Chem. Soc.*, 2011, **133**, 5668–5671.

62 G. Yu, B. Hua and C. Han, Proton transfer in host–guest complexation between a difunctional pillar[5]arene and alkyldiamines, *Org. Lett.*, 2014, **16**, 2486–2489.

63 P. Wei, X. Yan, J. Li, Y. Ma and F. Huang, Two 2:3 copillar[5]arene constitutional isomers: syntheses, crystal structures and host–guest complexation of derivatives with dicarboxylic acid sodium salts in water, *Chem. Commun.*, 2013, **49**, 1070–1072.

1426 | *Mater. Chem. Front.*, 2021, **5**, 1418–1427

This journal is © The Royal Society of Chemistry and the Chinese Chemical Society 2021

64 X. Hu, J. Hu, J. Tian, Z. Ge, G. Zhang, K. Luo and S. Liu, Cell-penetrating hyperbranched polyprodrug amphiphiles for synergistic reductive milieu-triggered drug release and enhanced magnetic resonance signals, *J. Am. Chem. Soc.*, 2013, **135**, 17617–17629.

65 V. Z. Sun, Z. Li, T. J. Deming and D. T. Kamei, Intracellular fates of cell-penetrating block copolypeptide vesicles, *Biomacromolecules*, 2011, **12**, 10–13.

66 X. Xue, S. Jin, C. Zhang, K. Yang, S. Huo, F. Chen, G. Zou and X.-J. Liang, Probe-inspired nano-prodrug with dual-color fluorogenic property reveals spatiotemporal drug release in living cells, *ACS Nano*, 2015, **9**, 2729–2739.

67 T. Xiao, L. Qi, W. Zhong, C. Lin, R. Wang and L. Wang, Stimuli-responsive nanocarriers constructed from pillar[n]arene-based supra-amphiphiles, *Mater. Chem. Front.*, 2019, **3**, 1973–1993.

68 G. Yu and X. Chen, Host–guest chemistry in supramolecular theranostics, *Theranostics*, 2019, **9**, 3041–3074.

69 M. J. Webber and R. Langer, Drug delivery by supramolecular design, *Chem. Soc. Rev.*, 2017, **46**, 6600–6620.

This journal is © The Royal Society of Chemistry and the Chinese Chemical Society 2021

Mater. Chem. Front., 2021, **5**, 1418–1427 | **1427**